Supplement of Atmos. Chem. Phys., 20, 13591–13610, 2020
https://doi.org/10.5194/acp-20-13591-2020-supplement

Atmospheric Chemistry and Physics
Open Access
EGU

Supplement of

Impacts of atmospheric transport and biomass burning on the inter-annual variation in black carbon aerosols over the Tibetan Plateau

Han Han et al.

Correspondence to: Jane Liu (janejj.liu@utoronto.ca)

1 GEOS-Chem evaluation

GEOS-Chem simulations of surface BC concentrations were previously evaluated over the TP and China (He et al., 2014; Li et al., 2016). Here, we validated the model in the TP and its surrounding regions for enhanced confidence. As surface BC measurements in the TP are rather limited, the observation data collected at 13 sites (Table S1 and Figure 1) from literature (Carrico et al., 2003; Qu et al., 2008; Zhang et al., 2008; Beegum et al., 2009; Ganguly et al., 2009; Bonasoni et al., 2010; Ming et al., 2010; Pathak et al., 2010; Ram et al., 2010a, b; Nair et al., 2012) were used in this study, following He et al. (2014). The 13 sites were grouped into urban, rural, and remote sites (He et al., 2014). The observational data are available for 2006 at 9 of the 13 sites and available at the other sites for different periods, i.e., 1999-2000, 2004-2005 and 2008-2009. BC observations at a remote site during 2015-2017 from another study (Chen et al., 2018) were also used.

The annual mean surface BC concentrations from GEOS-Chem and observations are compared in Table S1. The observed surface BC concentrations are below 2 μg m^{-3} at remote sites, about 2-5 μg m^{-3} at rural sites, and as high as 5 μg m^{-3} at urban sites (He et al., 2014). Compared with the observations, GEOS-Chem performs well at the remote sites, moderately at the rural sites, and poorly at the urban sites (Table S1). The simulations substantially underestimate surface BC concentrations at the urban sites, likely due to coarse horizontal resolution in the model that dilutes the intensity of local emissions in a model grid or due to higher BC emissions in 2006 than 2000. Taking the rural and remote sites only (Figure S1a), we found a high consistency between the annual mean simulations and observations, with a significant correlation coefficient of 0.99. The comparison suggests that GEOS-Chem can generally capture the spatial variation in surface BC concentrations over the TP. Moreover, the seasonality of simulated surface BC concentrations was evaluated at three sites (Figures S1b-S1d). GEOS-Chem simulates low BC concentrations in

summer and high BC concentrations in winter and spring at the sites. The amplitude of the seasonal variation in the simulations is weaker than that in the observations. Moorthy et al. (2013) found that simulated surface BC concentrations by the Goddard Global Ozone Chemistry Aerosol Radiation and Transport (GOCART) model in winter were lower than the observed ones at a TP site and they attributed this to the biases in the atmospheric boundary layer parameterization scheme. Wintertime surface BC concentrations were also underestimated by the Community Atmosphere Model version 5 (CAM5; Zhang et al., 2015), suggesting a common bias in these models.

We further compared surface BC concentrations from GEOS-Chem simulations with those from MERRA2 reanalysis (The Modern-Era Retrospective analysis for Research and Applications version 2, M2TMNXAER, https://cmr.earthdata.nasa.gov/search/concepts/C1276812866-GES_DISC.html; Figure S2 and Table S2). The magnitude and spatial distribution of BC concentrations in the TP from GEOS-Chem and MERRA2 are highly consistent, with correlation coefficients over 0.98 in the four seasons (Figure S2). BC concentrations from the two datasets show similar seasonality over most areas in the TP (Table S2). The interannual variations of surface BC over the TP during 1995-2014 from the two datasets have high similarity in spring, but the similarity is low in winter (Table S2). Furthermore, surface BC from the two datasets shows similar seasonal and interannual variations over East Asia, South Asia, and Southeast Asia, except for the interannual variation in winter (Table S2).

2 Characterizing the interannual variations in BC

We applied the mean absolute deviation (MAD) and absolute percent departure from the mean (APDM) to analyze the interannual variations in surface BC over the TP. The two indices can quantitatively represent the strength of the interannual variations

in BC (Mao and Liao, 2016). MAD and APDM are respectively calculated by Equations (S1) and (S2), where M_i is the surface BC concentrations averaged over the TP for year *i*, and *n* is the number of years (*n*=20 for 1995-2014). MAD and APDM represent the interannual variations of BC in terms of absolute value and percentage respectively. A higher MAD or APDM indicates a stronger variation.

$$MAD = \frac{1}{n}\sum_{i=1}^{n}\left|M_i - \frac{1}{n}\sum_{j=1}^{n}M_j\right| \quad \text{(S1)}$$

$$APDM = \frac{MAD}{\frac{1}{n}\sum_{i=1}^{n}M_i} \quad \text{(S2)}$$

Figure S4 shows the MAD and APDM of the surface BC concentrations in the TP. The MAD from CTRL simulation is highest in spring, being 0.019 μg m^{-3}, and is 0.007-0.008 μg m^{-3} in the other seasons (Figure S4a). The corresponding APDM values reach 73% in spring, and are around 30% in the other seasons (Figure S4b). Such seasonal patterns of the MAD and APDM show that the interannual variations of surface BC in the TP are strongest in spring. In spring, the MAD and APDM from FixBB simulation are much lower than those from CTRL simulation, while the MAD and APDM from FixMet simulation are comparable with those from CTRL simulation (Figure S4). This indicates that biomass burning plays an important role in driving the interannual variations of BC in spring. However, in summer, autumn and winter, the MAD and APDM from FixBB simulation are close to those from CTRL simulation (Figure S4). The MAD and APDM from FixMet simulation are small in summer, autumn, and winter. The comparison of MAD and APDM between the three simulations suggests that meteorology plays a larger role than biomass burning in driving the interannual variations of BC over the TP in these three seasons.

3 The emission perturbation simulation with GEOS-Chem

In order to make a comparison with the backward-trajectory method developed in this study, the emission perturbation method was applied to estimate the contributions of BC emissions in different source regions to surface BC in the TP. We conducted seven GEOS-Chem simulations, including one control experiment and six sensitivity experiments (Table S3). In the control experiment, all BC emissions were turned on. In the six sensitivity experiments, BC emissions from anthropogenic and fire sources are turned off individually in different source regions and in the entire world (Figure S5). The contribution of a region to surface BC in the TP can be represented by the difference in the BC amount between the control experiment and the corresponding sensitivity experiment for that region. The simulations were adjusted by a "normalized marginal" linearization method (Han et al., 2019). Figure S6 shows the contributions of BC emissions from central Asia, South Asia, East Asia, Southeast Asia, and the rest of world to surface BC in the TP.

In terms of the annual mean, BC emissions from South Asia (32%) and East Asia (50%) totally contribute to 82% of surface BC in the TP (Figure S6a). The contribution of South Asia to surface BC in the TP is higher in winter and spring than in summer and autumn. On contrast, the contribution of East Asia to surface BC in the TP is higher in summer and autumn. In the eastern TP, East Asia is the dominant source region of surface BC, with annual mean contributions of 77% (Figure S6b). South Asia is the dominant source region to surface BC in the southern, western, and central TP, with the annual mean contributions of 80%, 63%, 56% respectively for the three subregions (Figures S6c, S6d, and S6f). Central Asia contributes to over 46% surface BC in the northern TP (Figure S6e).

References

Beegum, S. N., Moorthy, K. K., Babu, S. S., Satheesh, S. K., Vinoj, V., Badarinath, K. V. S., Safai, P. D., Devara, P. C. S., Singh, S., Vinod, Dumka, U. C., and Pant, P.: Spatial distribution of aerosol black carbon over India during pre-monsoon season, Atmos. Environ., 43, 1071-1078, https://doi.org/10.1016/j.atmosenv.2008.11.042, 2009.

Bonasoni, P., Laj, P., Marinoni, A., Sprenger, M., Angelini, F., Arduini, J., Bonafè, U., Calzolari, F., Colombo, T., Decesari, S., Di Biagio, C., di Sarra, A. G., Evangelisti, F., Duchi, R., Facchini, MC., Fuzzi, S., Gobbi, G. P., Maione, M., Panday, A., Roccato, F., Sellegri, K., Venzac, H., Verza, GP., Villani, P., Vuillermoz, E., and Cristofanelli, P.: Atmospheric Brown Clouds in the Himalayas: first two years of continuous observations at the Nepal Climate Observatory-Pyramid (5079 m), Atmos. Chem. Phys., 10, 7515-7531, https://doi.org/10.5194/acp-10-7515-2010, 2010.

Carrico, C. M., Bergin, M. H., Shrestha, A. B., Dibb, J. E., Gomes, L., and Harris, J. M.: The importance of carbon and mineral dust to seasonal aerosol properties in the Nepal Himalaya, Atmos. Environ., 37, 2811-2824, https://doi.org/10.1016/S1352-2310(03)00197-3, 2003.

Chen, X., Kang, S., Cong, Z., Yang, J., and Ma, Y.: Concentration, temporal variation, and sources of black carbon in the Mt. Everest region retrieved by real-time observation and simulation, Atmos. Chem. Phys., 18, 12859-12875, https://doi.org/10.5194/acp-18-12859-2018, 2018.

Ganguly, D., Ginoux, P., Ramaswamy, V., Winker, D. M., Holben, B. N., and Tripathi, S. N.: Retrieving the composition and concentration of aerosols over the Indo-Gangetic basin using CALIOP and AERONET data, Geophys. Res. Lett., 36, L13806, https://doi.org/10.1029/2009GL038315, 2009.

Han, H., Liu, J., Yuan, H., Wang, T., Zhuang, B., and Zhang, X.: Foreign influences on tropospheric ozone over East Asia through global atmospheric transport,

Atmos. Chem. Phys., 19, 12495-12514, https://doi.org/10.5194/acp-19-12495-2019, 2019.

He, C., Li, Q. B., Liou, K. N., Zhang, J., Qi, L., Mao, Y., Gao, M., Lu, Z., Streets, D. G., Zhang, Q., Sarin, M. M., and Ram, K.: A global 3-D CTM evaluation of black carbon in the Tibetan Plateau, Atmos. Chem. Phys., 14, 7091-7112, https://doi.org/10.5194/acp-14-7091-2014, 2014.

Li, K., Liao, H., Mao, Y., and Ridley, A. D.: Source sector and region contributions to concentration and direct radiative forcing of black carbon in China, Atmos. Environ., 124, 351-366, https://doi.org/10.1016/j.atmosenv.2015.06.014, 2016.

Mao, Y.-H., and Liao, H.: Impacts of meteorological parameters and emissions on decadal, interannual, and seasonal variations of atmospheric black carbon in the Tibetan Plateau, Adv. Climate Change Res., 7, 123-131, https://doi.org/10.1016/j.accre.2016.09.006, 2016.

Ming, J., Xiao, C., Sun, J., Kang, S., and Bonasoni, P.: Carbonaceous particles in the atmosphere and precipitation of the Nam Co region, central Tibet, J. Environ. Sci., 22, 1748-1756, https://doi.org/10.1016/S1001-0742(09)60315-6, 2010.

Moorthy, K. K., Beegum, S. N., Srivastava, N., Satheesh, S. K., Chin, M., Blond, N., Babu, S. S., and Singh, S.: Performance evaluation of chemistry transport models over India, Atmos. Environ., 71, 210-225, https://doi.org/10.1016/j.atmosenv.2013.01.056, 2013.

Nair, V. S., Solmon, F., Giorgi, F., Mariotti, L., Babu, S. S., and Moorthy, K. K.: Simulation of South Asian aerosols for regional climate studies, J. Geophys. Res.-Atmos., 117, D04209, https://doi.org/10.1029/2011JD016711, 2012.

Pathak, B., Kalita, G., Bhuyan, K., Bhuyan, P. K., and Moorthy, K. K.: Aerosol temporal characteristics and its impact on shortwave radiative forcing at a location in the northeast of India, J. Geophys. Res.-Atmos., 115, D19204, https://doi.org/10.1029/2009JD013462, 2010.

Qu, W. J., Zhang, X. Y., Arimoto, R., Wang, D., Wang, Y. Q., Yan, L. W., and Li, Y.:

Chemical composition of the background aerosol at two sites in southwestern and northwestern China: potential influences of regional transport, Tellus B, 60, 657-673, https://doi.org/10.1111/j.1600-0889.2008.00342.x, 2008.

Ram, K., Sarin, M. M., and Hegde, P.: Long-term record of aerosol optical properties and chemical composition from a high-altitude site (Manora Peak) in Central Himalaya, Atmos. Chem. Phys., 10, 11791-11803, https://doi.org/10.5194/acp-10-11791-2010, 2010a.

Ram, K., Sarin, M. M., and Tripathi, S. N.: A 1 year record of carbonaceous aerosols from an urban site in the Indo-Gangetic Plain: Characterization, sources, and temporal variability, J. Geophys. Res.-Atmos., 115, D24313, https://doi.org/10.1029/2010JD014188, 2010b.

Zhang, R., Wang, H., Qian, Y., Rasch, P. J., Easter, R. C., Ma, P.-L., Singh, B., Huang, J., and Fu, Q.: Quantifying sources, transport, deposition, and radiative forcing of black carbon over the Himalayas and Tibetan Plateau, Atmos. Chem. Phys., 15, 6205-6223, https://doi.org/10.5194/acp-15-6205-2015, 2015.

Zhang, X. Y., Wang, Y. Q., Zhang, X. C., Guo, W., and Gong, S. L.: Carbonaceous aerosol composition over various regions of China during 2006, J. Geophys. Res.-Atmos., 113, D14111, https://doi.org/10.1029/2007JD009525, 2008.

Table S1. Comparison between observed and simulated annual mean surface BC concentrations (in μg m^{-3}) during the corresponding periods at various urban, rural, and remote sites (Figure 1a) over the TP and its surrounding regions.

Site category	Site name	Latitude (ºN)	Longitude (ºE)	Altitude (m)	Time period	Observations (μg m^{-3})	Simulations (μg m^{-3})	References
Remote	Nagarkot	27.7	85.5	2150	1999-2000	1.0	1.26	Carrico et al. (2003)
	NCOP	28.0	86.8	5079	2006	0.2	0.52	Bonasoni et al. (2010)
	Manora Peak	29.4	79.5	1950	2006	1.13	0.86	Ram et al. (2010a)
	NCOS	30.8	91.0	4730	2006	0.14	0.19	Ming et al. (2010)
	Langtang	28.1	85.6	3920	1999-2000	0.41	0.6	Carrico et al. (2003)
	Zhuzhang	28.0	99.7	3583	2004-2005	0.35	0.26	Qu et al. (2008)
Rural	Kharagpur	22.5	87.5	28	2006	5.56	4.45	Nair et al. (2012)
	Kanpur	26.4	80.3	142	2006	3.77	2.48	Ram et al. (2010b)
	Gandhi College	25.9	84.1	158	2006	4.88	4.05	Ganguly et al. (2009)
Urban	Delhi	28.6	77.2	260	2006	13.59	2.92	Beegum et al. (2009)
	Dibrugarh	27.3	94.6	111	2008-2009	8.91	1.13	Pathak et al. (2010)
	Lhasa	29.7	91.1	3663	2006	3.711	0.19	Zhang et al. (2008)
	Dunhuang	40.2	94.7	1139	2006	4.111	0.18	Zhang et al. (2008)

Table S2. Correlation coefficients of surface BC concentrations between GEOS-Chem simulations and MERRA2 reanalysis averaged over different regions. The abbreviations are for eastern TP (ETP), southern TP (STP), western TP (WTP), northern TP (NTP), central TP (CTP), central Asia (CAS), East Asia (EAS), South Asia (SAS), and Southeast Asia (SEAS).

	Seasonal variations	Interannual variations			
		Spring	Summer	Autumn	Winter
ETP	0.07	-0.22	0.21	0.62*	0.47*
STP	0.64*	0.33	0.31	0.37	0.16
WTP	0.47	0.89*	-0.16	-0.24	-0.4
NTP	0.66*	0.52*	0.50*	0.73*	0.01
CTP	0.72*	0.58*	0.06	-0.31	-0.32
CAS	-0.08	0.05	0.49*	0.7*	-0.02
EAS	0.94*	0.74*	0.68*	0.66*	0.31
SAS	0.95*	0.47*	0.63*	0.65*	0.32
SEAS	0.95*	0.75*	0.46*	0.41	0.72*

*The correlation coefficient is statistically significant ($p<0.05$).

Table S3. GEOS-Chem simulations conducted for estimating the contribution of different source regions to surface BC in the TP using the emission perturbation method[1].

Period	Experiment	Description
2005 (2004 for spin-up)	1. CTRL	Including all emissions
	2. E-GLO	Excluding global anthropogenic and fire emissions
	3. E-CAS	Excluding anthropogenic and fire emissions in CAS
	4. E-SAS	Excluding anthropogenic and fire emissions in SAS
	5. E-EAS	Excluding anthropogenic and fire emissions in EAS
	6. E-SEAS	Excluding anthropogenic and fire emissions in SEAS
	7. E-ROW	Excluding anthropogenic and fire emissions in ROW

[1]The abbreviations stand for different regions, including central Asia (CAS), South Asia (SAS), East Asia (EAS), and Southeast Asia (SEAS), and the rest of the world (ROW) (see Figure S5).

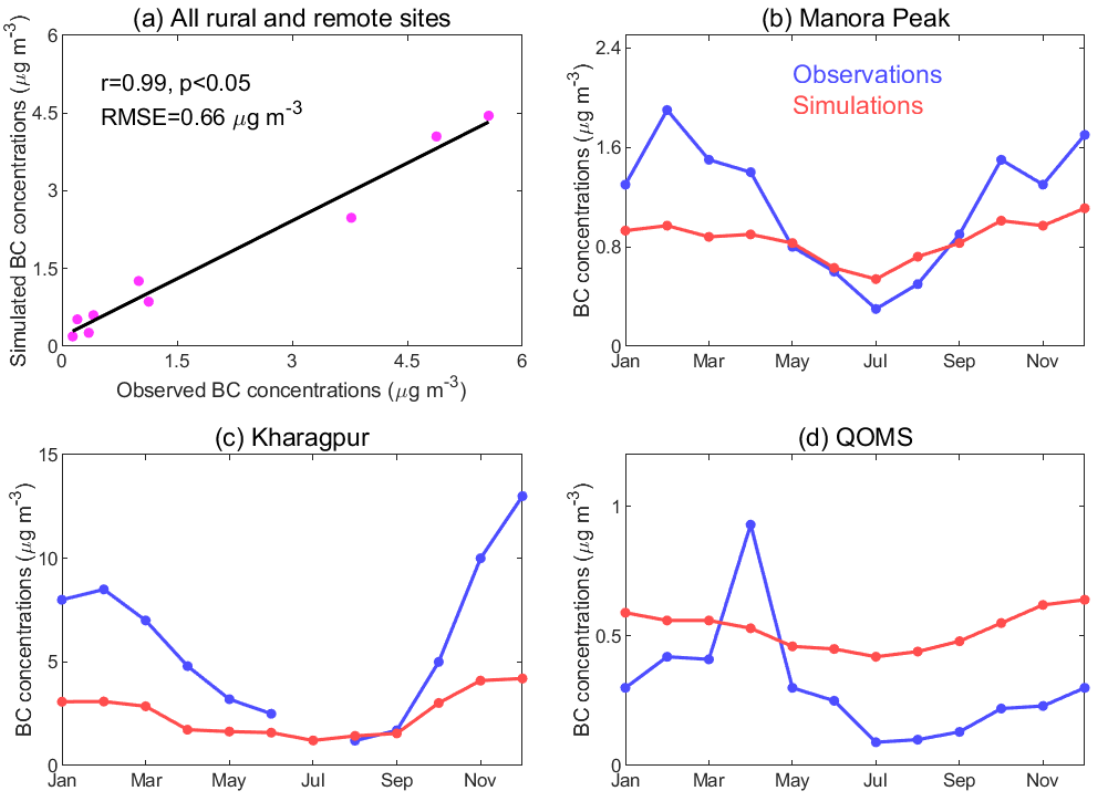

Figure S1. (a) Annual means of the observed and simulated surface BC concentrations at the rural and remote sites (see Table S1) in the TP and its surrounding regions in 2006. Comparisons between the monthly observations and simulations at (b) Manora Peak, (c) Kharagpur, and (d) QOMS (blue dots in Figure 1a) in 2006. Correlation coefficient (*r*) and root mean square error (RMSE) between the observed and simulated BC at all the rural and remote sites are also shown in (a). Observations at QOMS (28.36°N, 86.95°E, 4276 m) are from Chen et al. (2018).

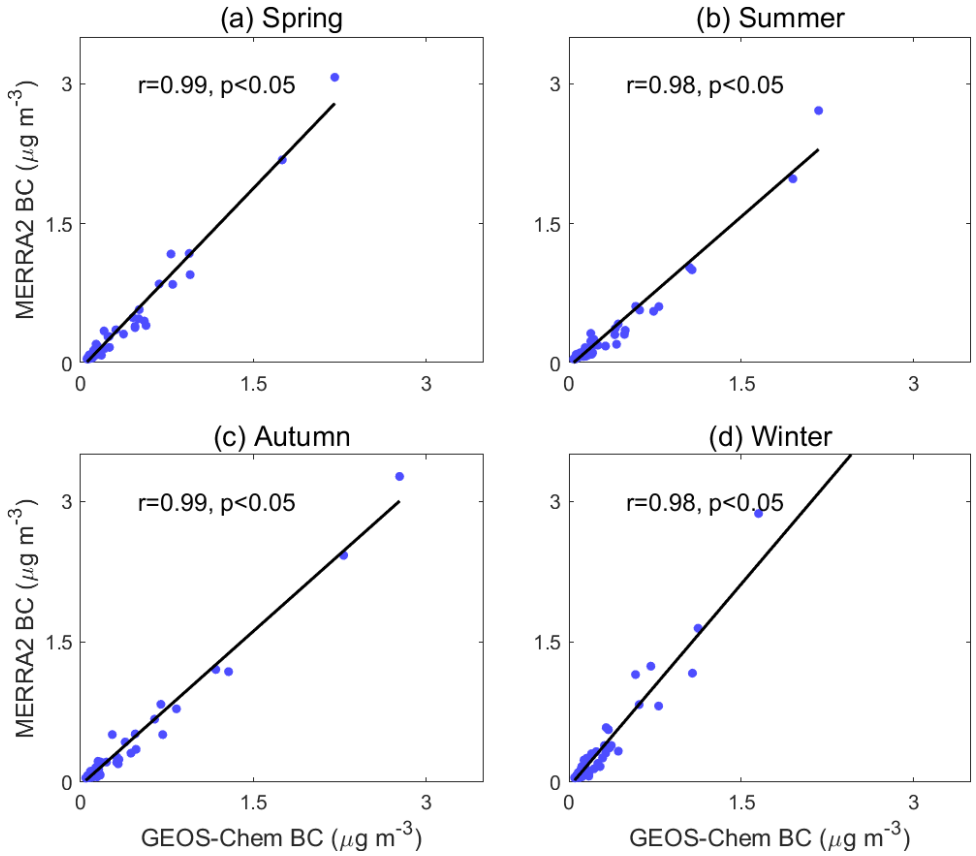

Figure S2. Comparison of surface BC concentrations between GEOS-Chem simulations and MERRA2 reanalysis at the 70 grids over the TP in the four seasons. The values are 20-year (1995-2014) means. The correlation coefficient (*r*) between the GEOS-Chem and MERRA2 BC concentrations and its significance level is shown in each panel.

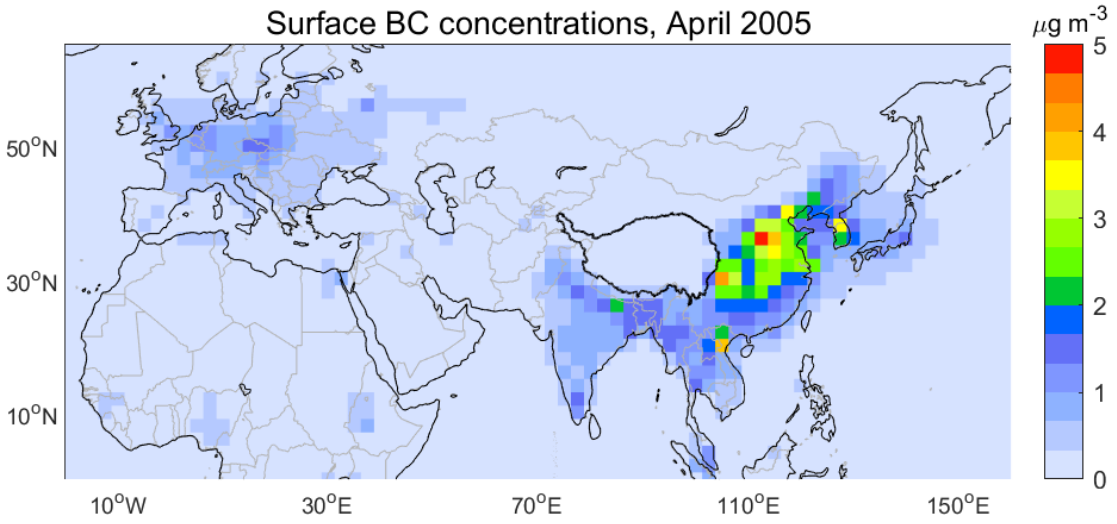

Figure S3. An example of GEOS-Chem simulated surface BC concentrations (in μg m^{-3}) in April 2005. The dark black line encloses the domain of the TP.

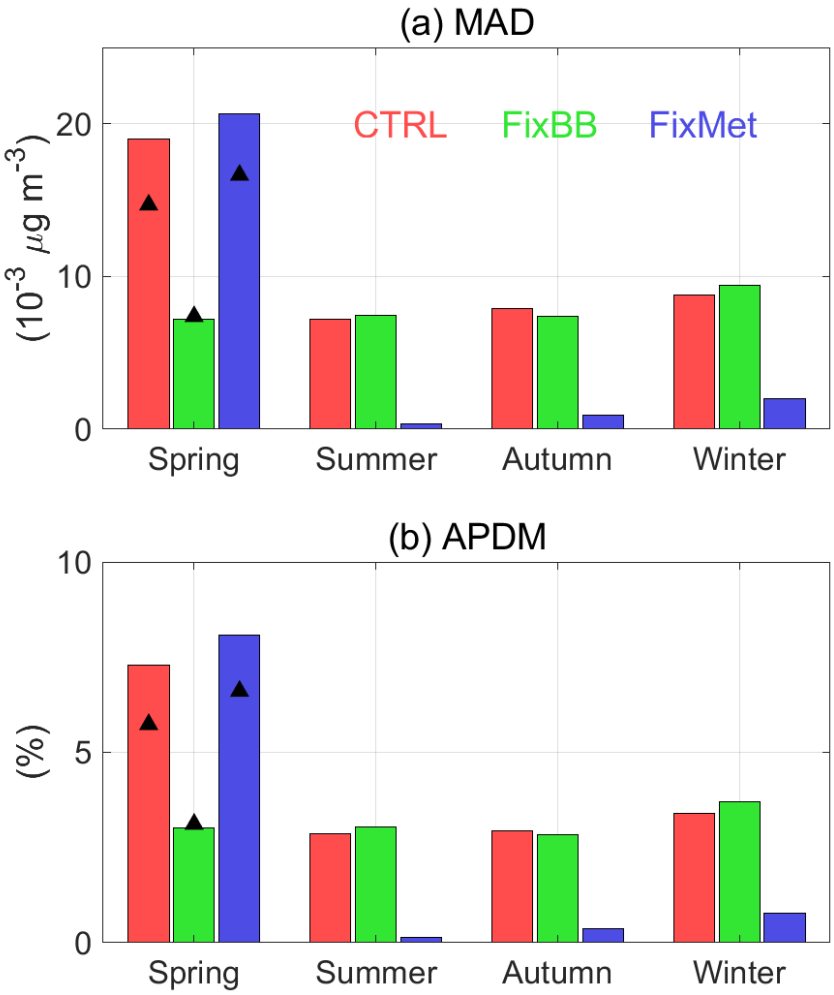

Figure S4. Mean absolute deviation (MAD) and absolute percent departure from the mean (APDM) of the simulated surface BC concentrations in the TP during 1995-2014. The triangles indicate the values calculated from simulations excluding the year 1999.

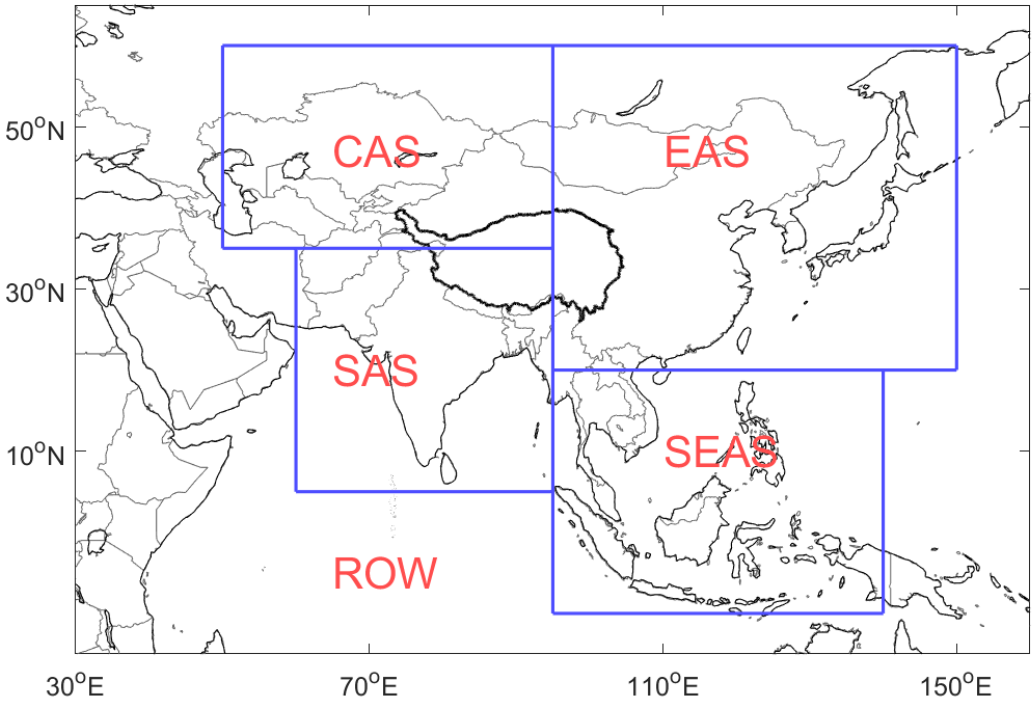

Figure S5. Regions defined for the emission perturbation method (Table S3). The regions include central Asia (CAS; 35-60°N, 50-95°E), East Asia (EAS; 20-60°N, 95-150°E), South Asia (SAS; 5-35°N, 60-95°E), Southeast Asia (SEAS; 10°S-20°N, 95-140°E), and the rest of the word (ROW). Note that the definitions of the regions used here are slightly different from those used for the backward-trajectory method in the main text.

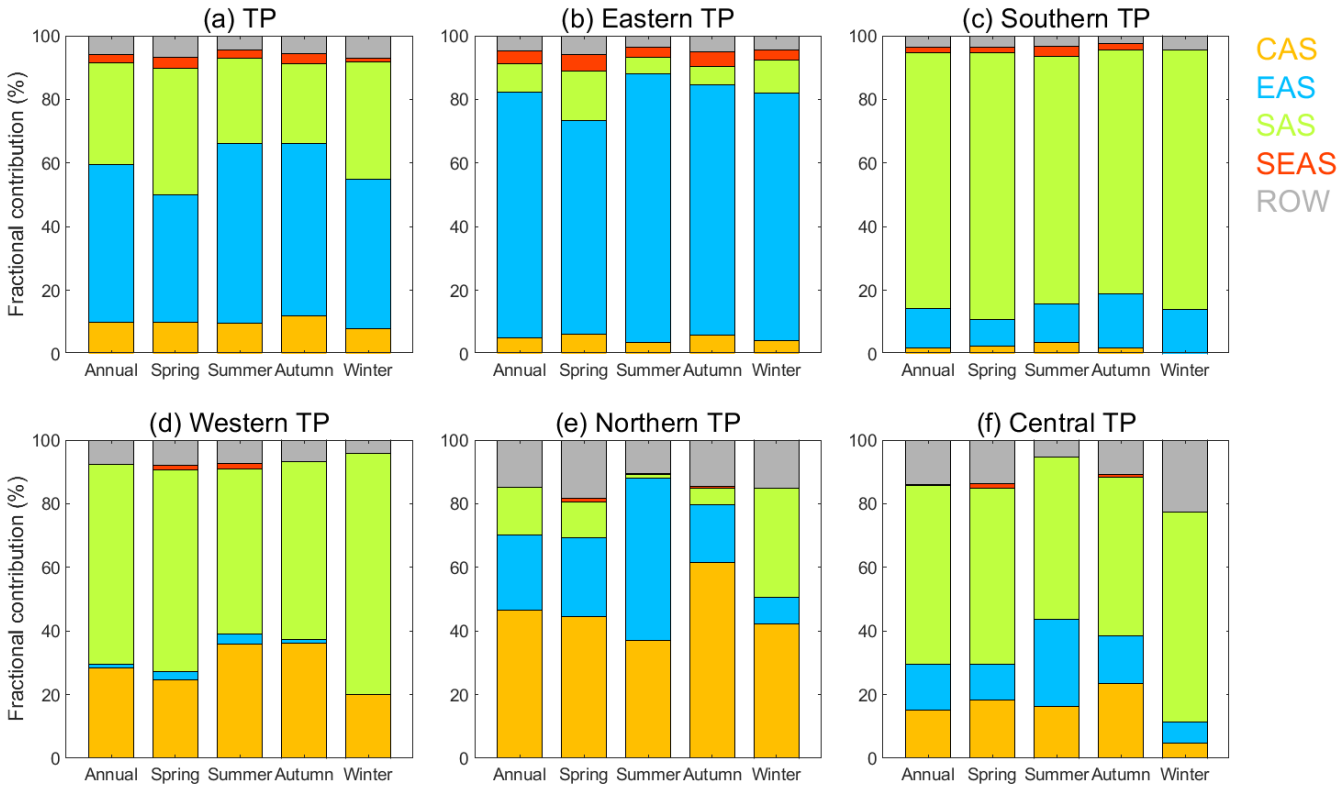

Figure S6. Fractional contributions of BC emissions from central Asia (CAS), South Asia (SAS), East Asia (EAS), Southeast Asia (SEAS), and the rest of the world (ROW) to surface BC over the TP and its subregions in 2005. The values are from the emission perturbation method using GEOS-Chem.

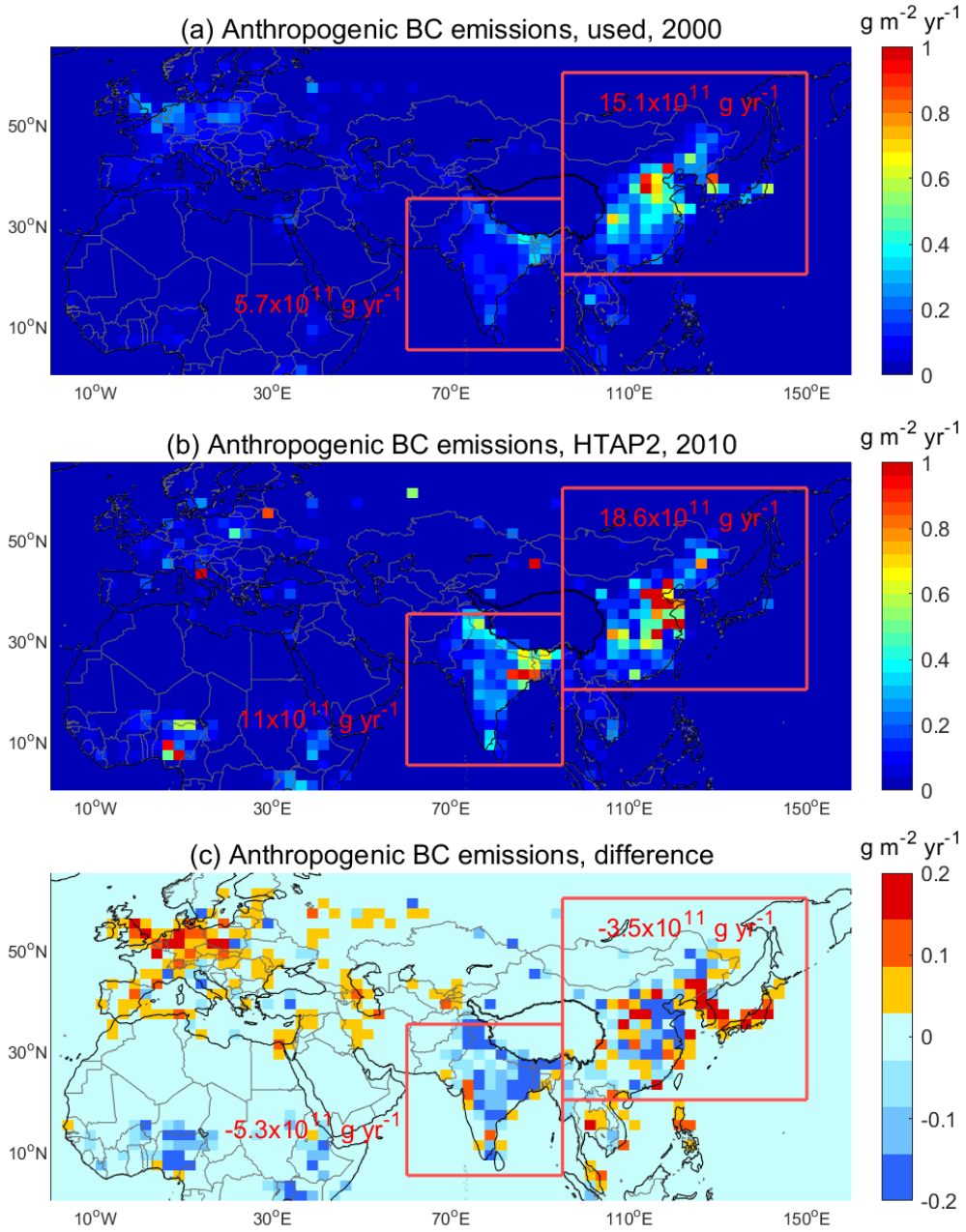

Figure S7. Anthropogenic BC emissions in the inventory used in GEOS-Chem for 2000 (a) and in the inventory for 2010 from the Task Force on Hemispheric Transport of Air Pollution Phase 2 (TF HTAP2) (b), and the difference between them (c). The red values are the regional means over the corresponding regions.